



Region-Based Convolutional Neural Nets for Localization of Glomeruli in Trichrome-Stained Whole Kidney Sections

John D. Bukowy ¹, Alex Dayton,¹ Dustin Cloutier,¹ Anna D. Manis,¹ Alexander Staruschenko ¹, Julian H. Lombard,¹ Leah C. Solberg Woods,² Daniel A. Beard,³ and Allen W. Cowley Jr.¹

¹Department of Physiology, Medical College of Wisconsin, Milwaukee, Wisconsin; ²Molecular Medicine, Wake Forest University School of Medicine, Winston-Salem, North Carolina; and ³Department of Molecular and Integrative Physiology, University of Michigan, Ann Arbor, Michigan

ABSTRACT

Background Histologic examination of fixed renal tissue is widely used to assess morphology and the progression of disease. Commonly reported metrics include glomerular number and injury. However, characterization of renal histology is a time-consuming and user-dependent process. To accelerate and improve the process, we have developed a glomerular localization pipeline for trichrome-stained kidney sections using a machine learning image classification algorithm.

Methods We prepared 4- μ m slices of kidneys from rats of various genetic backgrounds that were subjected to different experimental protocols and mounted the slices on glass slides. All sections used in this analysis were trichrome stained and imaged in bright field at a minimum resolution of 0.92 μ m per pixel. The training and test datasets for the algorithm comprised 74 and 13 whole renal sections, respectively, totaling over 28,000 glomeruli manually localized. Additionally, because this localizer will be ultimately used for automated assessment of glomerular injury, we assessed bias of the localizer for preferentially identifying healthy or damaged glomeruli.

Results Localizer performance achieved an average precision and recall of 96.94% and 96.79%, respectively, on whole kidney sections without evidence of bias for or against glomerular injury or the need for manual preprocessing.

Conclusions This study presents a novel and robust application of convolutional neural nets for the localization of glomeruli in healthy and damaged trichrome-stained whole-renal section mounts and lays the groundwork for automated glomerular injury scoring.

J Am Soc Nephrol 29: 2081–2088, 2018. doi: <https://doi.org/10.1681/ASN.2017111210>

The renal glomerulus, located at the proximal end of the nephron, is the site of bulk filtration of blood into tubular fluid. Progressive glomerular injury occurs in many disease states, including diabetes,¹ hypertension,^{2,3} and CKD.⁴ In studies of disease progression and its consequences, indices of glomerular injury serve as a powerful tool in assessing kidney function and damage. However, because of the number of nephrons within a kidney (approximately 30,000 in rats⁵ and approximately 1 million in humans⁶), assessing glomerular injury presents an arduous task fraught with issues related to

sample numbers and inter- and intraobserver variability. With the goal of reducing this burden, increasing sample sizes, and minimizing observer

Received November 21, 2017. Accepted May 17, 2018.

Published online ahead of print. Publication date available at www.jasn.org.

Correspondence: Dr. Allen W. Cowley Jr., Physiology, Medical College of Wisconsin, 8701 Watertown Plank Road, Milwaukee, WI 53226. Email: cowley@mcw.edu

Copyright © 2018 by the American Society of Nephrology

variability, this paper details the full automation of glomerular localization in both rat and human renal specimens, thereby laying the groundwork for automated glomerular injury scoring.

Previous studies within our department and others have used a glomerular injury index as a semiquantitative metric^{7–9} of overall glomerular injury in rat models. This index, as described by Raij *et al.*,¹⁰ seeks to quantify measures of GN, including mesangial expansion, open capillary lumen area, and fibrosis. The method has since been distilled to a scalar metric quantifying glomerular injury on a scale of zero to four (healthy to severely damaged). For a typical study, formalin-fixed kidneys are paraffin embedded and cut into 4- μ m-thick slices over either the short axis or long axis of the kidney. Staining with either Gömöri or Masson trichrome enhances cytoplasmic features in the tissue as well as fibrosis, an important marker of damage. For the 100–500 glomeruli that are observable in a single section, the common practice is to manually select and score a random sample of 60 cortical and 30 juxtamedullary glomeruli for a given biologic replicate.^{7–9} Although these methods provide an adequate sample size for determination of group differences, they are time consuming, are variable, and disregard spatial relationships between glomeruli.

Recently, there have been efforts to automate aspects of glomerular injury quantification. Sarder *et al.*¹¹ and more recently, Ginley *et al.*¹² described an unsupervised semiautomated workflow for localization and segmentation of glomerular features. Although their focus was on segmentation of features associated with glomeruli (Bowman's space, capillary lumen, *etc.*), they also described a color normalization and Gaussian blurring scheme to select glomerular candidates. Even using a limited sample size (15 fields with 148 glomeruli), an 87% localization accuracy was achieved, although the degree of glomerular injury was not reported. Additionally, their analysis simulated renal biopsy fields, and therefore, the robustness of this method when applied to whole kidney sections that include the morphologically distinctive medulla could not be determined.

Efforts have also been made using supervised machine learning for identification of glomeruli.^{13,14} A study by Marée *et al.*¹⁴ used 100 Masson trichrome–stained kidney slides with 2927 glomeruli and 13,648 nonglomerular structures to train their classifier, and it was validated on a similarly sized dataset. Images within the dataset were acquired using a Nanozoomer scanner (Hamamatsu Photonics, Hamamatsu City, Japan). The method achieved 95% precision and 81% recall in a binary classification task. Most recently, developments in the field of image processing have enabled image classification algorithms, specifically convolutional neural nets (CNNs), to gain traction in classifying histologic datasets.^{15,16} Pedraza *et al.*¹³ recently reported the first strides in using CNNs to classify “glomerulus” from “background” class objects using transfer learning from a pretrained version of Alexnet.¹⁷ Yet, although these methods can discriminate between images of glomeruli and “background” tissue, neither considers

Significance Statement

Histologic assessment of glomerular injury is widely used in both basic research and clinical practice to assess renal disease. Current methods require time-consuming manual localization of glomeruli, severely restricting the feasible number of observations from a given sample. Manual workflows also introduce both inter- and intra-observer variability as well as potential biases into the assessment. This paper presents the design and testing of a fully automated glomerular localization pipeline that is robust against biasing due to glomerular injury, enables high-throughput histologic phenotyping, permits quantification of the spatial distribution of glomerular injury, and ultimately, provides the framework for fully automated glomerular injury assessment in bright-field histology.

localization of glomeruli within a larger tissue region with multiple glomeruli present, limiting their utility in automated workflows. The localization of glomeruli in renal tissue is a necessary first step in the full automation of such histologic phenotyping workflows.

To address these current limitations, we have developed a glomerular localizer that consists of two serially arranged machine learning classifiers for automatic identification of glomeruli within whole kidney sections. The first stage is composed of a region-based convolutional neural net (R-CNN) for nominating glomerular candidates within wide-field images, and the second stage is a CNN for final classification of nominated candidates as either “glomerulus” or “background” objects. This method results in a localizer that can be used on whole kidney sections with average precision of 96.94% and 80.2% and average recall of 96.79% and 81.67% for rat and human kidneys, respectively. Additionally, in a subset of rat kidneys, we show no evidence for biasing of the localizer for glomerular injury. Furthermore, as demonstration of a localizer use case, we generate and examine glomerular depth profiles for a set of genetically crossed and mapped heterogeneous rat stock. With these profiles, we provide evidence for separation of glomerular depth profiles between animals that may be used to isolate a genetic locus for encoding for glomerular depth. Finally, we provide tools for investigators to score glomeruli in a semiautomated manner using the modified scale by Raij *et al.*¹⁰ These methods permit a description of spatial relationships between glomeruli in whole kidney sections, a semiautomated scoring pipeline, and a means to generate large datasets for future automation of injury classification.

METHODS

Specimens

The training dataset is composed of whole rat kidney slices from various experimental protocols unrelated to this study. The dataset includes a mixture of kidneys that were either flushed with saline before collection or left unaltered (22 flushed and 52 nonflushed). The genetic background of the

samples differed and included inbred Dahl SS (SS/JrHsdMcwi) as well as outbred heterogeneous stock as reported by Solberg Woods *et al.*¹⁸ These rat strains, particularly the heterogeneous stock with wide genetic variation, were chosen to maximize the diversity of kidney morphology for training and testing.

Two sets of Masson-stained kidney tissue were set aside from the training dataset for testing purposes. Set 1 included 13 additional rat kidneys, and set 2 included six human samples of whole renal tissue including both cortical and medullary regions. Renal sections contained varying degrees of glomerular and tubular injury. All animal protocols were approved by the Medical College of Wisconsin Institutional Animal Care and Use Committee. Human tissue was from deidentified patients and obtained from the Medical College of Wisconsin Tissue Bank.

Histologic Preparation and Imaging

Kidneys were fixed in 10% formalin and saved for batch processing depending on experimental preparation. For histologic staining, kidneys were paraffin embedded, sectioned at 4 μm , and stained with either Gömöri or Masson trichrome. Imaging was performed on either a Nikon Ni-E automated microscope in red, green, and blue color at 0.68 μm per pixel (20 \times equivalent) or a Nanozoomer with images extracted at 0.92 μm per pixel (10 \times equivalent).

Histologic slices used for glomerular distance to surface measurements were taken from midsectional slices. This was done to control for any measurement error that may have been introduced from kidney geometry or slice angle.

Color Deconvolution and Virtual Stain Separation

Stain separation was achieved using color deconvolution.¹⁹ Color basis vectors were automatically solved using an adaptation of the method described by Macenko *et al.*²⁰ and implemented in MATLAB 2017a (The Mathworks Inc., Natick, MA). Principal component analysis was performed on each pixel using features described by its OD, red, green, and blue color space, and hue, saturation, and value color space values. The first two principal components were plotted, and the angle with respect to the first principal component was found for each pixel. OD color basis vectors were resolved from the angle covering the first and 99th percentiles of the plotted observations.

Color deconvolution was performed using the solved color basis vectors. Intensity images were created for the “red” and “blue” stain components. Histogram equalization was then performed on the extracted “red” layer over only tissue-related pixels with background removed through masking. These stain-separated and normalized grayscale images were then retained for dataset creation.

Ground Truth Dataset Creation

With color deconvoluted and normalized grayscale images, the “ground truth” glomerular locations (gold standard: assessed by a trained human observer) in our analysis were manually defined using the MATLAB Training Image Labeler.

Nonoverlapping scenes (1500 \times 1500 pixels) were obtained from each whole kidney section. Rectangular regions of interest were then drawn around glomeruli within each scene, excluding those with an estimated 25% or less visible area within the field (at image borders). This resulted in a training dataset with 23,540 glomerular observations. The testing dataset was created from manual identification of 5447 glomeruli on a subset of kidneys excluded from training. To assess biasing due to injury, manual glomerular scoring was performed by a single observer on a subset of rat kidneys included in both the training and testing datasets (20 and three kidneys, respectively).

CNN Design and Training

Two serially arranged classifiers were implemented to localize glomeruli within the kidney sections. The CNN structure was on the basis of the previously described Alexnet¹⁷ modified to accept grayscale images (227 \times 227 pixels) and predict the input image as either “glomerulus” or “background.” Finally, training started with the pretrained weights from Alexnet as implemented in MATLAB 2017a. The first pass was trained using the MATLAB 2017a implementation of fasterRCNN²¹ with the full training dataset with a learning rate of 0.0001 for approximately 65 epochs (approximately 65,000 iterations). The fully trained R-CNN was rerun on the entire set of training data, and the resulting candidate proposals were manually sorted into a secondary training dataset. The probability threshold associated with the output from the R-CNN was adjusted to obtain an equal number of “background” and “glomerulus” class observations. A base instance of our modified Alexnet architecture was then trained on the secondary training dataset that included approximately 22,000 glomeruli and approximately 22,000 background images for the second pass CNN. The CNN was trained with batch sizes of 10,000 images and a learning rate of 0.0001 for 1200 epochs (6000 iterations) (Supplemental Figures 1 and 2).

RESULTS

Image Dataset and Preprocessing

The aim of this workflow was to automate glomerular localization for the assessment of injury and associated phenotypes. Trichrome staining, commonly used to assess glomerular injury, enhances tissue/cellular features and fibrotic signals, but using a signal associated with injury for glomerular localization has a high potential for biasing the localizer. To reduce biasing due to injury and decrease variance due to staining, images of whole kidney sections underwent preprocessing and normalization before localization.

To minimize signals due specifically to fibrosis, an automated method for virtual stain separation was implemented (Methods). In short, by using a large number of observations (pixels) (Figure 1A) that have varying contributions from two different stains, a stain signature for each can be extracted that

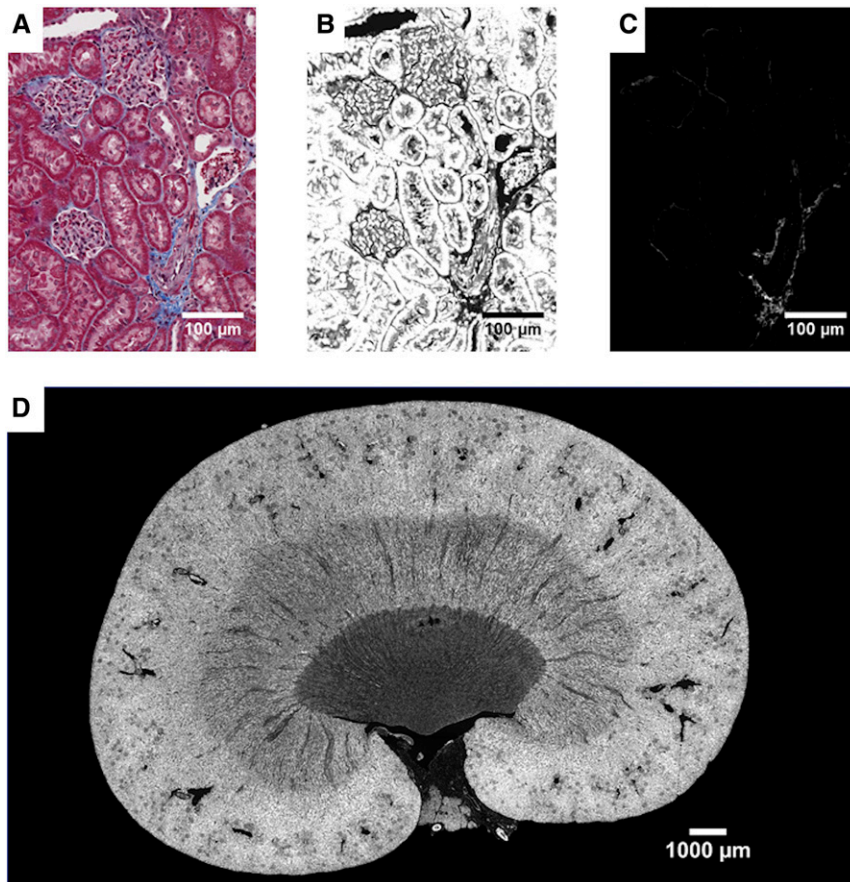


Figure 1. Color normalization process virtually separates stains to normalize tissue samples and decrease signal associated with fibrosis. (A) Color deconvolution vectors were extracted from this subset of pixels using a method adapted from Macenko *et al.*²⁰ To decrease computation time, a small region with “pure” examples of red and blue staining was selected from the larger image. Color deconvolution vectors were solved for each renal section. (B and C) After deconvolving, the original image with color vectors derived from (A) virtual stain separation approximated (B) red stain contribution from (C) blue stain contribution. (D) Using only the grayscale image associated with the red staining, histogram equalization was performed over the tissue section, increasing contrast for glomerular detection (dark puncta near surface).

describes the amount of stain 1 and stain 2 associated with a given pixel. Color deconvolution was then performed using these signatures, resulting in separate intensity images related to the amount of each stain present. In our workflow, the grayscale image associated with the red staining (cytoplasm) (Figure 1B) is saved for localization, whereas the image associated with blue staining (fibrosis) (Figure 1C) is discarded. Finally, histogram equalization was performed on the red stain-associated grayscale image to enhance contrast. The resulting images emphasize the distinctive glomerular morphology as dark puncta near the surface (Figure 1D).

Glomerular Localization Workflow Training and Testing

Using the preprocessed images, training and testing datasets were created. As indicated in Methods, an R-CNN was

implemented that placed box outlines around glomerular candidates within an imaged field and assigned a probability of each candidate belonging to class “glomerulus” or “background.”

Initial training of this R-CNN was performed using 72 whole kidney sections processed into smaller nonoverlapping blocks. Bounding boxes for 23,540 glomeruli were manually assigned by a human observer in 4791 blocks. After approximately 65,000 iterations, training accuracy averaged 92.45%.

The fully trained R-CNN was then rerun on these same 72 training set kidney sections to localize glomeruli. Glomerular candidates from the second pass were manually sorted into two classes: “glomerulus” or “background.” An inclusion probability for each glomerular candidate was adjusted to create a secondary training dataset consisting of 44,122 observations equally split between “glomerulus” and “background” classes. This resulted in a secondary training dataset that was enriched for background examples with a high misclassification rate to provide better training examples. With training on the secondary dataset, the CNN achieved an average training accuracy of 99.22%.

Testing was then performed on the fully trained ensemble classifier. The test dataset was created from 13 whole kidney sections containing 5447 glomeruli, where the center location of each glomerulus was manually annotated. True positives were defined by a >50% overlap of the predicted region with a 150×150-pixel region centered over the manually annotated glomerulus (cyan boxes in Figure 2, A and C). False positives

and false negatives were defined similarly (red boxes and magenta boxes, respectively, in Figure 2, A and C). True negatives were not recorded. In rare instances where glomeruli appeared in close proximity (estimated <1% of observations), the classifier bound both glomeruli within the same region of interest. In this case, our performance metric would represent both glomeruli as found; however, only a single bounding box (observation) would be recorded. This could potentially lead to a discrepancy between the predicted glomerular count and true count. Regardless, precision and recall were assessed for the full localizer by adjusting a single threshold parameter (Figure 2B [rat] and Figure 2D [human]), resulting in average precision and recall of 96.94% and 96.79%, respectively, for the rat (Figure 2B, Inset) and average precision and recall of 80.2% and 81.67%, respectively, for human samples (Figure 2D,

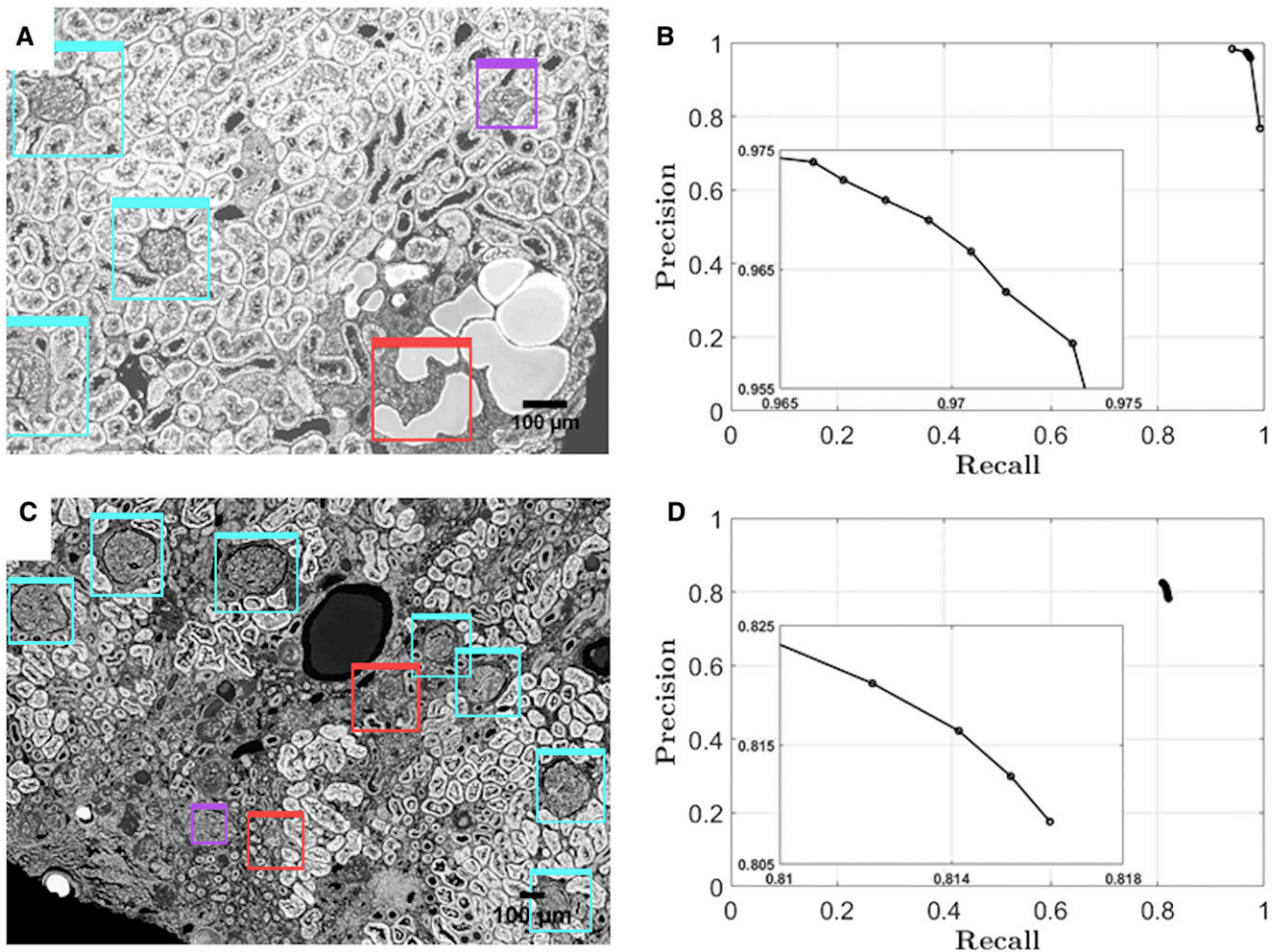


Figure 2. Testing of localizer and proposed workflow shows high precision and recall in rat and human test data. (A) Example scene of a rat kidney within the test set. Cyan boxes denote true positives or where there is >50% overlap of the predicted region of interest with a ground truth box of 150×150 pixels placed over the center of a glomerulus. Magenta boxes show false negatives and show relative size of the ground truth bounding box. Red boxes show false positives or where the algorithm incorrectly identified background tissue as a glomerulus. The representative field shows the variability of glomerular injury and tubular damage. (B) Precision-recall curve of all observations within the test dataset (5447 glomeruli). Values were achieved by sweeping the probability threshold associated with glomerular candidate output of the trained region-based convolutional neural net. (Inset) Magnified precision-recall curve with probability threshold between 0.86 and 0.92. (C) Example scene of a human kidney within the expanded test set, with examples of glomerular and tubular injury. Color code is identical to that in A. (D) Precision-recall curve for all human observations within the expanded test set (1173 glomeruli). (Inset) Magnified precision-recall curve with probability threshold between 0.88 and 0.94.

Inset). The localizer's reduced performance on the human tissue is attributed to differences in size and appearance between rat and human glomeruli. However, the human results are still remarkable considering complete omission of human data from the training set. Refinements to the localizer's performance on human tissue could be made by expanding the training dataset with human samples.

Evaluation of Detector Bias Associated with Assigned Glomerular Injury Score

This localizer will ultimately be used for automated assessment of glomerular injury in health and disease. Therefore, biasing of the localizer for either injured or healthy glomeruli is an

important design consideration. To evaluate bias of the detector toward healthy or injured glomeruli, detector performance was evaluated on a subset of the test dataset where glomerular injury had been assessed by a trained observer on a scale of zero to four as previously reported.^{7–9} Representative examples of injured glomeruli and their corresponding scores are provided in Supplemental Figure 3. Kidneys ($n=3$) from the scored subset had an average glomerular injury score of 2.54 ± 0.26 (from scores assigned to approximately 90% of the glomeruli). An example field is presented in Figure 2A.

In total, this subset included 735 glomeruli. Table 1 shows the distribution of glomerular injury. The three kidneys were processed with the fully trained localizer, and false negatives

Table 1. Evaluation of localizer bias to glomerular injury score: False negative rate contingency table

Renal Injury	False Negative	Ground Truth	Percentage	Fisher Exact
Score 0	0	0	—	$P=0.46$
Score 1	0	5	0	
Score 2	13	438	2.97	
Score 3	5	271	1.85	
Score 4	0	21	0	
Total	18	735	2.45	

Within the test set, three rat kidneys were evaluated for glomerular injury on the basis of the modified semiquantitative scale by Raji *et al.*¹⁰ Approximately 90% of glomeruli from these kidneys were assessed for glomerular injury (example scored images are in Supplemental Figures 1–3). Of the kidneys assessed for injury, the test set was constructed from the most injured examples, thereby providing an extreme injury test case for the detector. The dataset was evaluated with the trained localizer with a threshold of 0.90. The distribution of false negatives from the detector was limited to scores of two and three, coinciding with the highest score populations in the test set. Using a Fisher exact test, the prevalence of missing one score class over another was not found to be statistically significant. This is consistent with a lack of bias toward glomerular injury from the localizer. —, is undefined.

that had injury score assignments were recorded. These false negatives were also included in the contingency table sorted by their associated renal injury score. A Fisher exact test was

performed to assess bias in the score population where false negatives occurred. From this analysis, we found no evidence that the localizer had a bias toward missing glomeruli of any given score ($P=0.46$).

Characterizing Glomerular Depth Profiles

One application of the developed methods includes characterization of glomerular depth profiles. Figure 3 presents a group of midline whole kidney sections from 16 individual rats of the heterogeneous stock. For each of these animals, glomerular position results from the localizer were used to construct a histogram describing the distance of glomerulus from the renal surface (see supplement S1 for renal surface estimation method). Figure 3A is a three-dimensional plot of these histograms (normalized to total observations to create an empirical probability distribution function). The colors pertain to the probability of a glomerulus appearing within this depth. The histograms are ordered by skewness (“lean” of a fit log-normal distribution). This highlights the weighting of each histogram for superficial glomeruli. Figure 3B displays two cumulative probability distributions of the log-normal distribution fits for the extreme cases presented in Figure 3A. The 95% confidence intervals of these fits are then plotted using

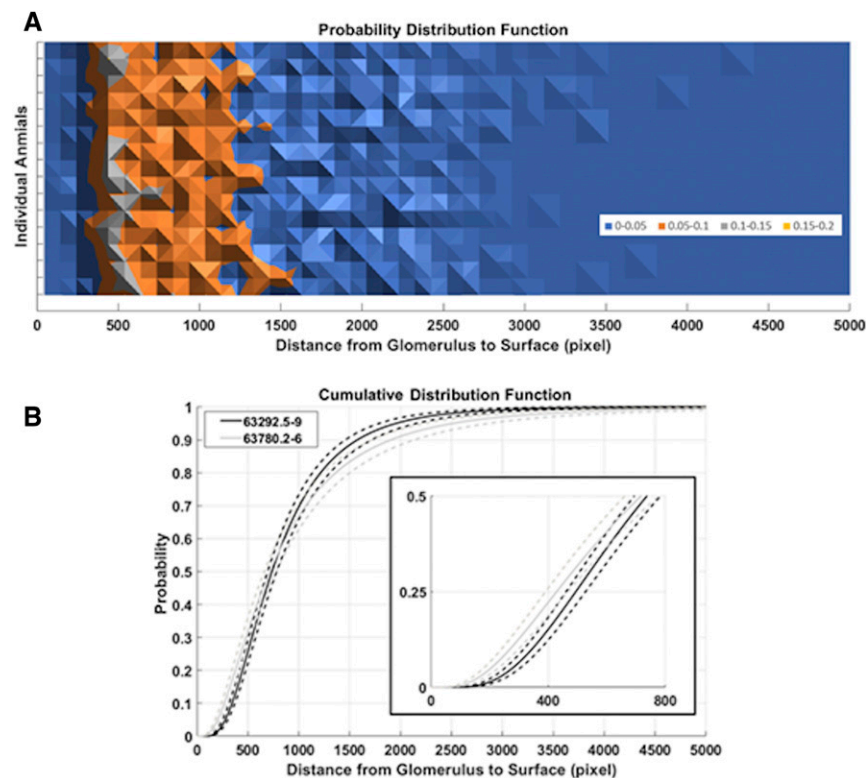


Figure 3. Characterization of distance from renal surface to glomeruli within whole kidney sections shows separation between individuals in heterogeneous rat stock. (A) Empirically determined probability distribution functions describing the probability of a glomerulus given a distance from the renal surface. Sixteen individual rats are plotted in order of skewness from least to most (top to bottom). Skewness describes the “lean” of a probability density function. (B) Cumulative distribution functions of log-normal distributions fit to the two extreme animals of plot A (top row [gray line]; bottom row [black line]). The dashed lines show the 95% confidence intervals. Inset shows cumulative distribution functions from 0% to 50% probability.

the dotted lines in Figure 3B. This indicates that, in this given dataset, there appears to be a statistically significant skewing of the log-normal probability distribution functions. The analysis was, therefore, able to statistically separate glomerular depth profiles of individual rats within the heterogeneous stock and provides a proof of concept that these metrics can be used to compare glomerular depths between genetically distinct animals.

DISCUSSION

A summary diagram of the training, testing, and ultimate production use of this localizer is presented in Figure 4. To our knowledge, the dataset presented here (28,987 rat glomeruli) represents the largest published dataset for the training and testing of glomerular localization in histologic images. Large sample sizes are imperative for use in both training and testing to avoid overfitting of the classifier and subsequent overestimation of classifier performance. Sample size alone can contribute more to classifier performance than the specific classifier method used.²² Importantly, we have also assessed an index of glomerular injury in a subset of the data showing a diverse population of glomeruli for training and testing. This process has not only provided training cases to improve classifier

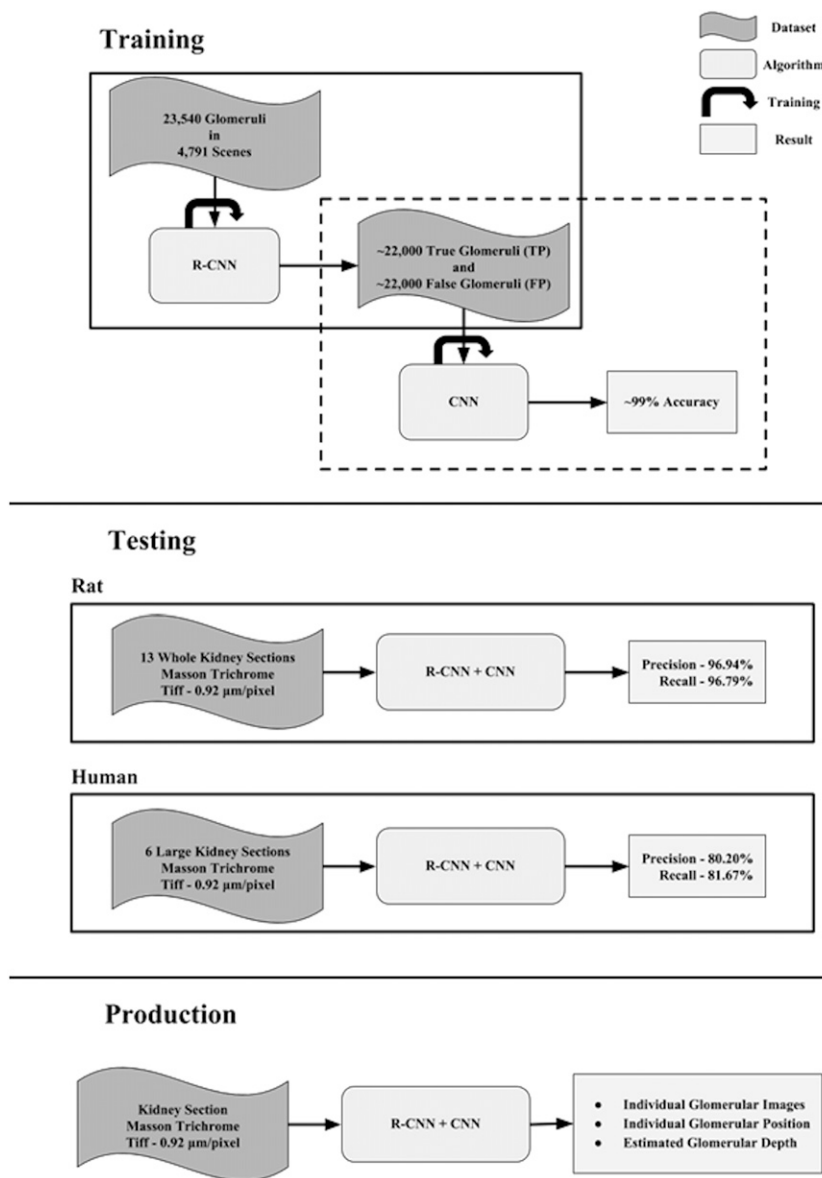


Figure 4. Training, testing, and production workflow of the described glomerular localizer. Training describes the datasets used for the total training of the classifiers. Solid and dashed outlines show separate training efforts. The output from the region-based convolutional neural network (R-CNN) was used for training of the secondary convolutional neural network (CNN). When the training dataset for the CNN was enriched with examples that the first-stage R-CNN failed to identify correctly, the secondary classifier becomes more robust against errors. Training of the localizer was performed solely on rat tissue specimens but provides impressive localization on human kidney samples.

performance over the range of glomerular injury but also, permitted estimation of bias in the classifier for healthy or damaged glomeruli.

Pedraza *et al.*¹³ recently published a CNN algorithm to sort previously cropped images into the two separate classes. They achieved an excellent 99.95% with tenfold crossvalidation on an augmented dataset (700 observations per class original and 5300 observations per class augmented). These results,

however, relied on manual cropping of the images against manually selected negative observations. Although this is a fair assessment of sorting previously human-cropped images of glomeruli, our desired workflow requires localization of glomeruli within a scene—a much different task. Our method not only classifies whether a given candidate belongs to class “glomerulus” or “background” but also, implements a region proposal algorithm to localize glomeruli within the context of an entire kidney cross-section.

Previous studies using simulated renal biopsies^{11,12} show no examples for inclusion of the distinctive medullary tissue. With early iterations of our glomerular localizer using whole kidney sections with the trained R-CNN workflow, we obtained an unacceptable false positive rate within the medulla, likely due to the presence of high-intensity nuclei resembling glomeruli. This problem was a consequence of hardware limitations that restricted the maximum scene size that could be used for training. This, in turn, limited examples of negative data from the medulla. This problem was circumvented by enriching the training dataset for difficult images and training a secondary CNN to further improve classification. This design resulted in the method described above, which is robust against all of the renal tissue types visible within whole kidney sections.

In addition to vetting our classifier against renal sections that include medullary tissue, we also examined the consequence of glomerular injury on localization performance, an important consideration for glomerular injury assessment on naive datasets. A subset of glomeruli within the ground truth dataset was assessed for injury, thereby providing a unique twofold advantage to our method. First, the localizer was trained on a dataset known to include glomeruli with a diverse population of renal injury scores. Second, misclassification as a function of glomerular injury was quantified showing no evidence for bias in the localizer for or against severely injured glomeruli. Because of the heterogeneity observed in glomerular histology, it is essential that the localizer remain unbiased against degree of injury or variation in morphology.

In summary, the method that we have developed provides an automated tool for localization of healthy and diseased glomeruli (see supplement S2 for proposed pipeline and

end-user tools). It enables a multitude of analysis pipelines that were previously too laborious to perform on a routine basis. Dissector/Fractionator methods²³ that rely on glomerular positioning between sections become trivial when combined with whole-kidney sections registration. Additionally, by resolving the location of every observable glomerulus and subsequently assigning glomerular injury scores, spatial injury clustering analysis can be performed, enabling a new high-throughput phenotype. The method not only represents an improvement in precision and recall over previously published works but also, provides a robust solution that does not require further parameterization.

ACKNOWLEDGMENTS

This research was completed in part with computational resources and technical support provided by the Research Computing Center at the Medical College of Wisconsin.

This study was supported by National Institutes of Health (NIH) grants HL-116264 (to A.W.C.) and HL-122662 (to A.W.C.). The heterogeneous stock rat colony was supported by NIH grant R01 DK088975 (to L.C.S.W.). J.D.B. is funded by American Heart Association predoctoral fellowship grant AHA16PRE29700006. Contributions from D.C. and J.H.L. were supported by NIH grants R01 HL-128242 and R21 OD024781.

DISCLOSURES

None.

REFERENCES

- Kakimoto T, Okada K, Hirohashi Y, Relator R, Kawai M, Iguchi T, et al.: Automated image analysis of a glomerular injury marker desmin in spontaneously diabetic Torii rats treated with losartan. *J Endocrinol* 222: 43–51, 2014
- Evans LC, Petrova G, Kurth T, Yang C, Bukowy JD, Mattson DL, et al.: Increased perfusion pressure drives renal T-cell infiltration in the dahl salt-sensitive rat. *Hypertension* 70: 543–551, 2017
- Kumar V, Wollner C, Kurth T, Bukowy JD, Cowley AW Jr.: Inhibition of mammalian target of rapamycin complex 1 attenuates salt-induced hypertension and kidney injury in dahl salt-sensitive rats. *Hypertension* 70: 813–821, 2017
- Venkatachalam MA, Griffin KA, Lan R, Geng H, Saikumar P, Bidani AK: Acute kidney injury: A springboard for progression in chronic kidney disease. *Am J Physiol Renal Physiol* 298: F1078–F1094, 2010
- Bertram JF, Soosaipillai MC, Ricardo SD, Ryan GB: Total numbers of glomeruli and individual glomerular cell types in the normal rat kidney. *Cell Tissue Res* 270: 37–45, 1992
- Nyengaard JR, Bendtsen TF: Glomerular number and size in relation to age, kidney weight, and body surface in normal man. *Anat Rec* 232: 194–201, 1992
- Cowley AW Jr., Yang C, Zheleznova NN, Staruschenko A, Kurth T, Rein L, et al.: Evidence of the importance of Nox4 in production of hypertension in dahl salt-sensitive rats. *Hypertension* 67: 440–450, 2016
- Evans LC, Ryan RP, Broadway E, Skelton MM, Kurth T, Cowley AW Jr.: Null mutation of the nicotinamide adenine dinucleotide phosphate-oxidase subunit p67phox protects the Dahl-S rat from salt-induced reductions in medullary blood flow and glomerular filtration rate. *Hypertension* 65: 561–568, 2015
- Spurgeon-Pechman KR, Donohoe DL, Mattson DL, Lund H, James L, Basile DP: Recovery from acute renal failure predisposes hypertension and secondary renal disease in response to elevated sodium. *Am J Physiol Renal Physiol* 293: F269–F278, 2007
- Raij L, Azar S, Keane W: Mesangial immune injury, hypertension, and progressive glomerular damage in Dahl rats. *Kidney Int* 26: 137–143, 1984
- Sarder P, Ginley B, Tomaszewski JE: Automated renal histopathology: Digital extraction and quantification of renal pathology. Presented at the SPIE, San Diego, CA, March 23, 2016
- Ginley B, Tomaszewski JE, Sarder P: Automatic computational labeling of glomerular textural boundaries. In: SPIE Medical Imaging, Orlando, FL, International Society for Optics and Photonics, 2017
- Pedraza A, Gallego J, Lopez S, Gonzalez L, Laurinavicius A, Bueno G: Glomerulus classification with convolutional neural networks. In: Annual Conference on Medical Image Understanding and Analysis, edited by Hernández MV, González-Castro V, Springer, 2017, pp 839–849
- Marée R, Dallongeville S, Olivo-Marin J-C, Meas-Yedid V: An approach for detection of glomeruli in multisite digital pathology. Presented at the 2016 IEEE 13th International Symposium on Biomedical Imaging (ISBI), 2016, pp 1033–1036
- Esteve A, Kuprel B, Novoa RA, Ko J, Swetter SM, Blau HM, et al.: Dermatologist-level classification of skin cancer with deep neural networks. *Nature* 542: 115–118, 2017
- Temerinac-Ott M, Forestier G, Schmitz J, Hermesen M, Bräseni J, Feuerhake F, et al.: Detection of glomeruli in renal pathology by mutual comparison of multiple staining modalities. Presented at the 2017 10th International Symposium on Image and Signal Processing and Analysis (ISPA), 2017, pp 19–24
- Krizhevsky A, Sutskever I, Hinton GE: Imagenet classification with deep convolutional neural networks. *Adv Neural Inf Process Syst*, 2012, pp 1097–1105
- Solberg Woods LC, Holl K, Tschannen M, Valdar W: Fine-mapping a locus for glucose tolerance using heterogeneous stock rats. *Physiol Genomics* 41: 102–108, 2010
- Ruifrok AC, Johnston DA: Quantification of histochemical staining by color deconvolution. *Anal Quant Cytol Histol* 23: 291–299, 2001
- Macenko M, Niethammer M, Marron J, Borland D, Woosley JT, Guan X, et al.: A method for normalizing histology slides for quantitative analysis. Presented at the 2009 ISBI'09 IEEE International Symposium on Biomedical Imaging: From Nano to Macro, 2009, pp 1107–1110
- Ren S, He K, Girshick R, Sun J: Faster R-CNN: Towards real-time object detection with region proposal networks. *Adv Neural Inf Process Syst*, 2015, pp 91–99
- Banko M, Brill E: Scaling to very very large corpora for natural language disambiguation. Presented at the 39th Annual Meeting on Association for Computational Linguistics, 2001, pp 26–33
- Cullen-McEwen LA, Douglas-Denton RN, Bertram JF: Estimating total nephron number in the adult kidney using the physical dissector/fractionator combination. *Methods Mol Biol* 886: 333–350, 2012
- Chan TF, Vese LA: Active contours without edges. *IEEE Trans Image Process* 10: 266–277, 2001

See related editorial, "AI: What Have You Done for Us Lately?," on pages 2031–2032.

This article contains supplemental material online at <http://jasn.asnjournals.org/lookup/suppl/doi:10.1681/ASN.2017111210/-/DCSupplemental>.